Electronic Supplementary Information (ESI)

Reaction Site Exchange in Hierarchical Bimetallic Mn/Ni Catalyst Triggered by Electron Pump Effect to Boost Urea Electrocatalytic Oxidation

Yajun Song, [†a] *Zhijiao Ji,* [†a] *Shenghao Zhao,* [a] *Tianqi Wang,* [a] *Jia Liu,* [a,b,e *] *and Wenping Hu* [a,c,d]

[a] Tianjin Key Laboratory of Molecular Optoelectronics, Department of Chemistry, School of Science, Tianjin University,Tianjin, 300072 (P. R. China)

[b] Key Laboratory of Advanced Energy Materials Chemistry (Ministry of Education), College of Chemistry, Nankai University, Tianjin 300071, People's Republic of China

[c] Collaborative Innovation Center of Chemical Science and Engineering (Tianjin), Tianjin 300072, People's Republic of China.

[d] Joint School of National University of Singapore and Tianjin University, Fuzhou International Campus, Tianjin University, Binhai New City, Fuzhou, 350207, People's Republic of China.

[e] Yulin University, Yulin, 719000, Shanxi Province, People's Republic of China.

† Yajun. Song, and Zhijiao. Ji contributed equally to this work.

* Corresponding authors: E-mail: liujia@tju.edu.cn

1. Methods Section

1.1 Synthesis of Ni-BDC nanosheets

The Ni-BDC nanosheets were synthesized following the previously reported method with slight modifications.[1] In a typical synthesis, 1,4-benzenedicarboxylic acid (BDC) (0.15 mmol) and $NiCl_2 \cdot 6H_2O$ (0.15 mmol) were first dissolved in the mixed solution of N, N-Dimethylformamide (DMF) (13 mL), ethanol (800 μL), and water (800 μL) at room temperature and constant stirring for 30 min to form a homogeneous solution. The solution was then transferred into a 25 mL stainless steel autoclave lined with Teflon and maintained at 140 °C for 48 h. Finally, the sample was removed from the oven and

cooled to room temperature. The obtained light green products were washed with DMF, deionized water, and ethanol several times and dried in the vacuum oven at 60 °C overnight.

1.2 Synthesis of NiS_2 nanospheres

First, Ni-BDC nanosheets (20 mg) and thioacetamide (TAA) (100 mg) were dissolved into 15 mL ethanol at a mass ratio of 1:5 to form a homogeneous solution. After stirring for 30 min, the mixture was transferred into a stainless steel autoclave lined with Teflon and maintained at 160 °C for 6 h. The obtained products were washed with deionized water and ethanol several times and dried in a vacuum at 60 °C overnight. Finally, the NiS_2 nanospheres were obtained.

1.3 Synthesis of L-NiS_2@MnO_x and S-NiS_2@MnO_x nanocomposites

NiS_2@MnO_x nanocomposites were synthesized by liquid (1) and solid (2) phase methods.

(1) First, NiS_2 (10 mg) nanospheres were ultrasonically dissolved in 8 mL of deionized water. Then, under magnetic stirring, a certain amount of $KMnO_4$ was added to the solution, and the mixture was stirred for 4 hours. The mass ratio of NiS_2 to $KMnO_4$ were 5:1, 10:1, 15:1, 20:1 respectively, and these samples were named as L-NiS_2@MnO_x-1, L-NiS_2@MnO_x-2, L-NiS_2@MnO_x-3, L-NiS_2@MnO_x-4. After the reaction, the products were washed several times with deionized water and ethanol and then dried in a vacuum at 60 °C overnight. Finally, the L-NiS_2@MnO_x nanocomposite materials were obtained.

(2) NiS_2 (10 mg) and a certain amount of $KMnO_4$ were placed in a mortar and ground for 30 min. The mass ratios of NiS_2 to $KMnO_4$ were 5:1, 10:1, 15:1, 20:1, respectively, and these samples were named as S-NiS_2@MnO_x-1, S-NiS_2@MnO_x-2, S-NiS_2@MnO_x-3, S-NiS_2@MnO_x-4. The obtained black powder was washed several times with deionized water and ethanol and dried in a vacuum at 60 °C overnight. Finally, the S-NiS_2@MnO_x nanocomposite materials were obtained.

1.4 Synthesis of CoS_2@MnO_x

The method for preparing CoS_2@MnO_x was the same as for preparing NiS_2@MnO_x, except that $NiCl_2 \cdot 6H_2O$ was replaced by $CoCl_2 \cdot 6H_2O$.

1.5 Synthesis of M-NiS_2@MnO_x nanocomposites

NiS_2 (10 mg) and a certain amount of MnO_2 were weighed and placed in a mortar and ground for 30 min. The obtained black powder was washed several times with deionized water and ethanol and dried in a vacuum at 60 °C overnight. Finally, the M-NiS_2@MnO_x nanocomposite material was obtained.

1.6 Physical characterization

The crystal structure of the sample was characterized by powder X-ray diffraction (XRD, Rigaku SmartLab 9 KW). The surface morphology and composition of the material were characterized by a field emission scanning electron microscope (FESEM, Hitachi, SU8010). Transmission electron microscope (TEM) images were obtained by JEM-JEOL2100F. The DXR2xi Raman imaging microscope was used to record the Raman spectra under 633 nm laser excitation. The X-ray photoelectron spectroscopy (XPS) signals were obtained with a Thermo ESCALAB 250xi system with an Al Ka X-ray monochromator.

1.7 Preparation of working electrode

Electrocatalytic inks were prepared using mixing catalyst, dispersant, and Nafion 117 solution. First, disperse 2 mg of catalyst in 200 μL of dispersant ethanol, then 20 μL Nafion 117 solution (0.5%) was added, ultrasonic treatment for more

than 1.5 hours until the catalyst was completely dispersed and uniform. Finally, 50 μL of catalyst ink was directly dripped on a clean carbon paper (~ 1.0 cm × 1.2 cm) and placed at room temperature overnight to dry. After electrocatalytic testing, the working electrode was washed with clean water and dried at room temperature for other physical characterization such as SEM, XRD, and XPS.

1.8 Electrocatalytic urea oxidation (UOR)

The electrochemical test was carried out in a three-electrode system using the electrochemical workstation of Shanghai Chenhua Instrument Co. Ltd. The catalyst loaded carbon paper was used as the working electrode (WE), Hg/HgO and carbon rod electrode were used as reference electrode (RE) and counter electrode (CE), respectively. All potentials were calibrated against the reversible hydrogen electrode by the following formula:

E (RHE) = E (Hg / HgO) + 0.059 × pH + 0.098.

All electrochemical tests were performed at room temperature. First, the working electrode was activated by cyclic voltammetry (CV) in 1 M KOH solution until the signal was stable. Then the electrocatalytic urea oxidation experiment was carried out. Because the concentration of urea in human urine is about 0.33 M,[2, 3] and most of the currently published literature chose this concentration for experiments. Therefore, UOR were carried out in the electrolyte of 1.0 M KOH and 0.33 M urea. The linear sweep voltammetry (LSV) curves were all recorded when the sweep rate was 5 mV s^{-1}.

The electrochemical active surface area (ECSA) of the catalyst can be calculated from the double-layer capacitance value (C_{dl}). The double-layer capacitance value of the material was obtained from the CV diagram in the non-Faraday range, and its potential window range was 0.976~1.076 V (vs. RHE). Cyclic voltammetry was performed in 1 M KOH solution with scan rates of 20, 40, 60, 80, and 100 mV s^{-1}. The double-layer capacitance value can finally be estimated by plotting the ratio of current density to scan rate at 1.05 V (vs. RHE).

The electrochemical impedance spectroscopy (EIS) test was carried out in the frequency range of 0.1 Hz ~ 100 kHz in1 M KOH and 0.33 M urea at the potential of 1.32 V (vs. RHE). The stability of the material was analyzed by the Chronoamperometric method, which was conducted at 1.34 V (vs. RHE) for 90000 s. 1.7. DFT calculation

1.8 Calculation of TOF values for catalyst

The calculation of the turnover frequency (TOF) value, which was calculated using the following formula:

$$TOF = \frac{jA}{6nN_A e} = \frac{jA}{6nF}$$

The density j (mA cm^{-2}) at 1.5 V (vs. RHE) was chosen to calculate the amount of charge each metal site can provide, and the electrode surface area A was about 1 cm^{-2}. The current required to convert one urea molecule is $6e^-$. F is Faraday's constant (96485 C/mol), and n is the number of moles of metal atoms. On the working electrode, the mass (m) of the material is 0.5 mg. The actual proportion of Mn in the material as determined by ICP-MS. We using Mn as the active site to calculate the TOF of L-NiS_2@MnO_2.

2. DFT calculation Section

When carried out DFT calculation, gradient approximation (GGA) method with Perdew-Burke-Ernzerhof (PBE) functional were employed.3 The van der Waals interactions were estimated by using DFT-D3 method with.4 Energy cut-off was set to 400 eV. The NiS_2 (0 0 1) surfaces with (3 × 3× 3) cell, MnO_2 (0 1 0) and (0 0 1) surfaces with(2 × 2× 2) cell were modeled, and Gamma k-point was adopted. A vacuum space of 10 Å in the z-direction was set to minimize

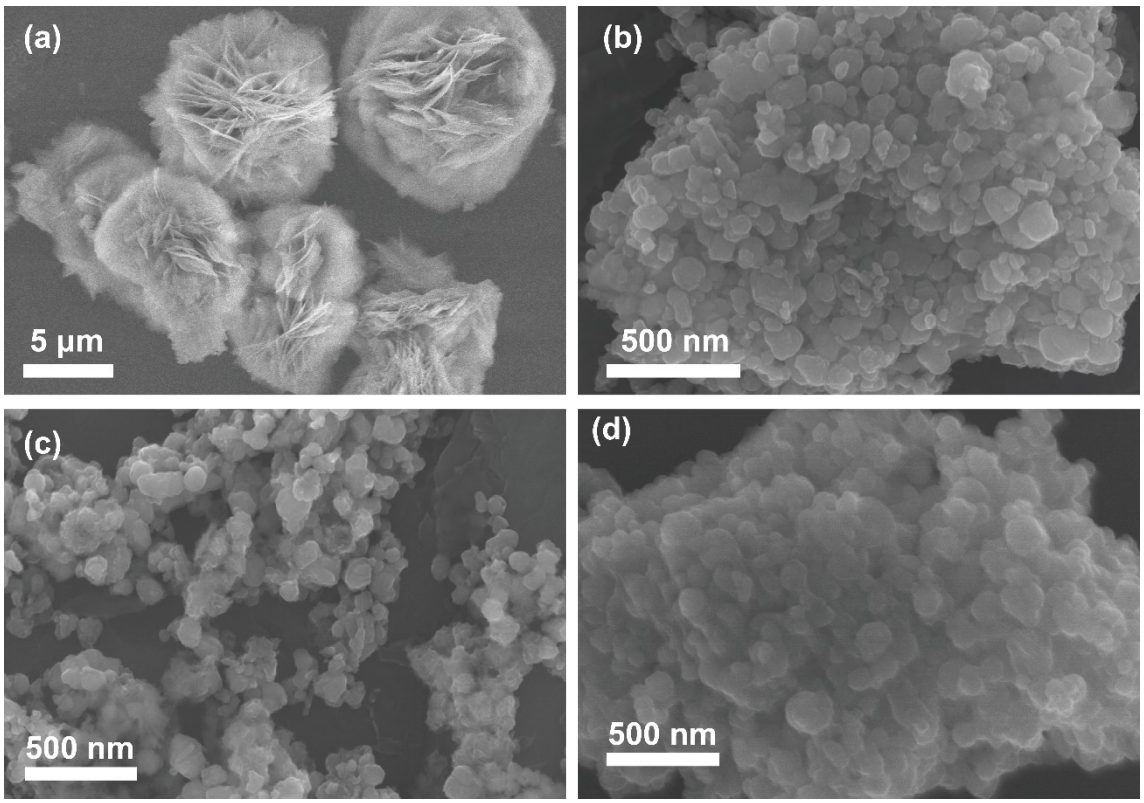

interactions among neighboring substrate images. The atoms of top layer were fully relaxed to optimize the thermodynamic stable structure. The adsorption energy (ΔE) is the electronic energy difference directly obtained from DFT calculations, ΔZPE is the change in zero-point energies, T is the temperature (T =298.15 K), and ΔS is the entropy change.

Figure S1. SEM images of (a) Ni-BDC, (b) NiS_2, (c) L-NiS_2@MnO_x-3, and (d) S-NiS_2@MnO_x-2.

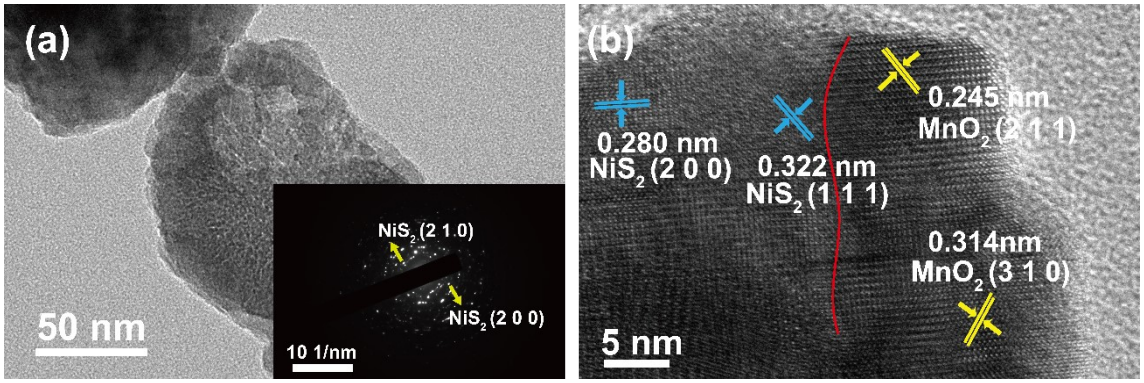

Figure S2. (a) HRTEM image of S-NiS_2@MnO_x-2.Inset: SAED pattern of S-NiS_2@MnO_x-2. (b) Partially enlarged HRTEM of S-NiS_2@MnO_x-2.

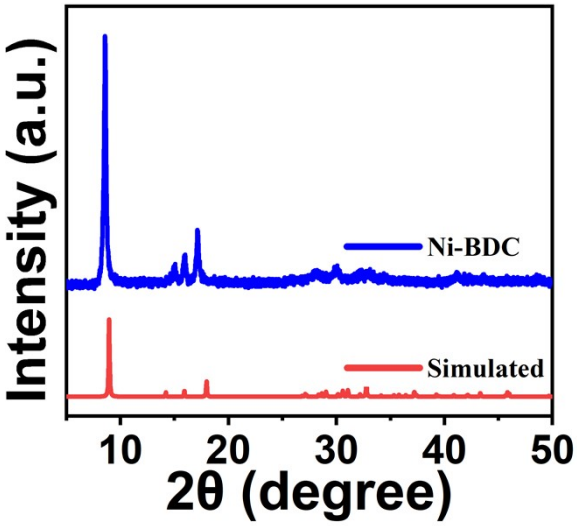

Figure S3. XRD patterns of Ni-BDC.

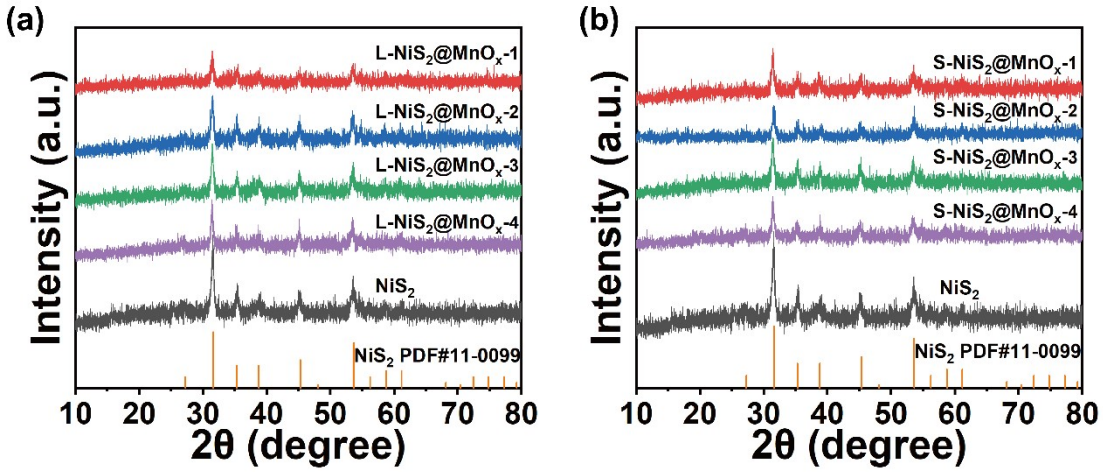

Figure S4. XRD patterns of (a) NiS_2 and L-NiS_2@MnO_x-n, (b) NiS_2 and S-NiS_2@MnO_x-n.

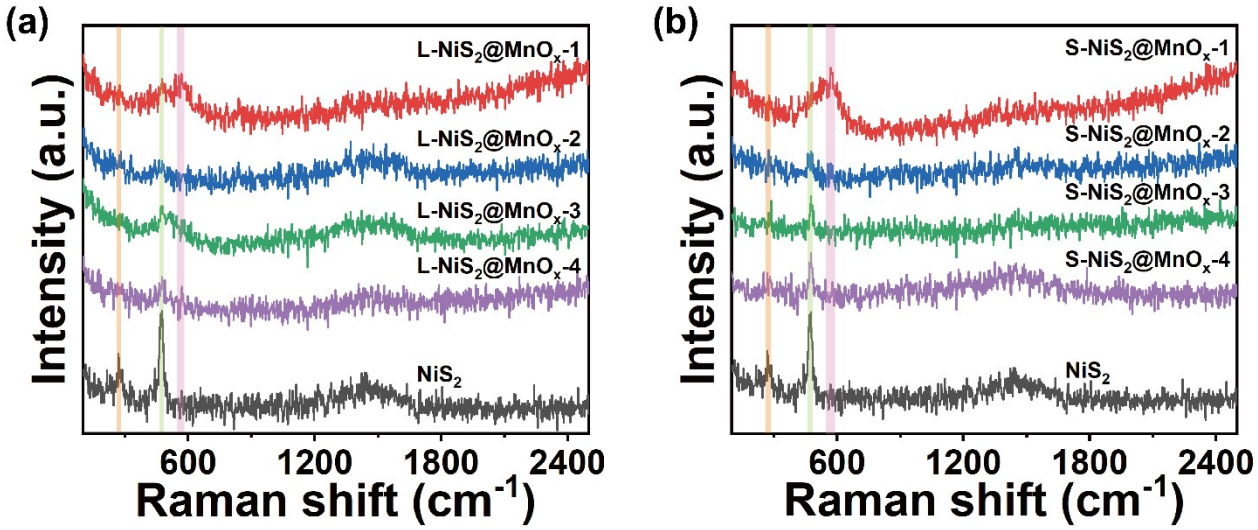

Figure S5. Raman spectra of (a) NiS_2 and L-NiS_2@MnO_x-n, (b) NiS_2 and S-NiS_2@MnO_x-n.

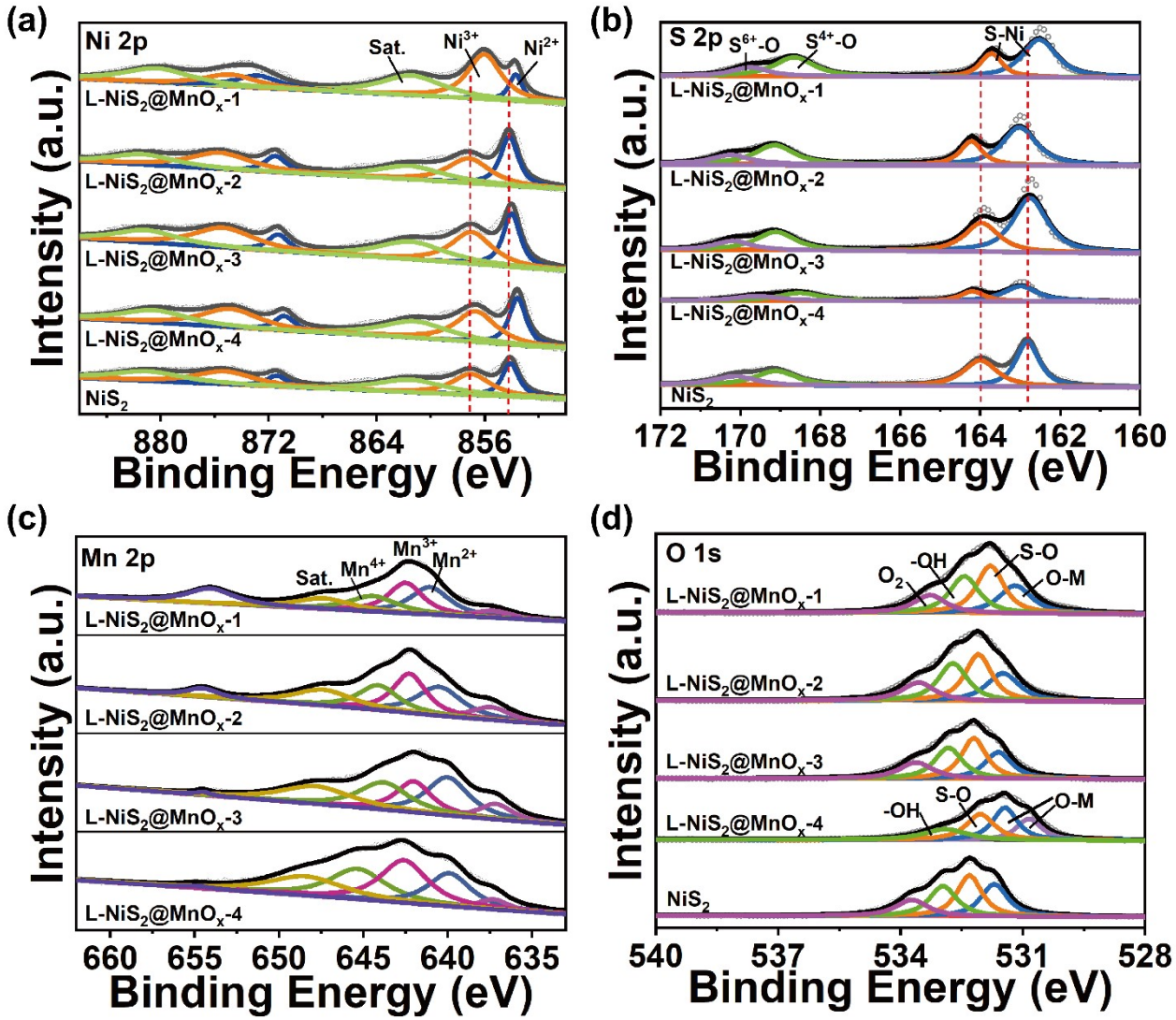

Figure S6. XPS spectra of (a) Ni 2p, (b) S 2p, (c) Mn 2p, and (d) O 1s of NiS_2 and L-NiS_2@MnO_x-n.

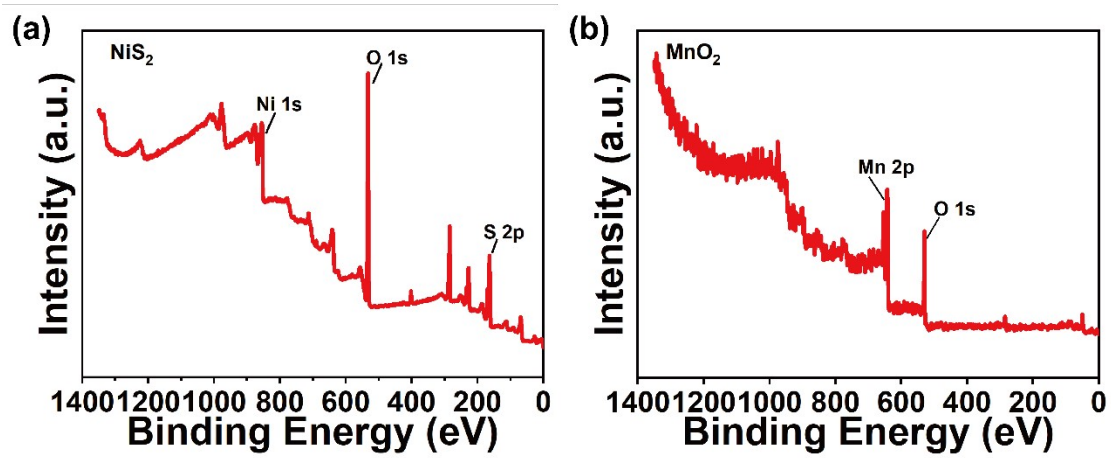

Figure S7. Full XPS spectra of (a) NiS_2 and (b) MnO_2.

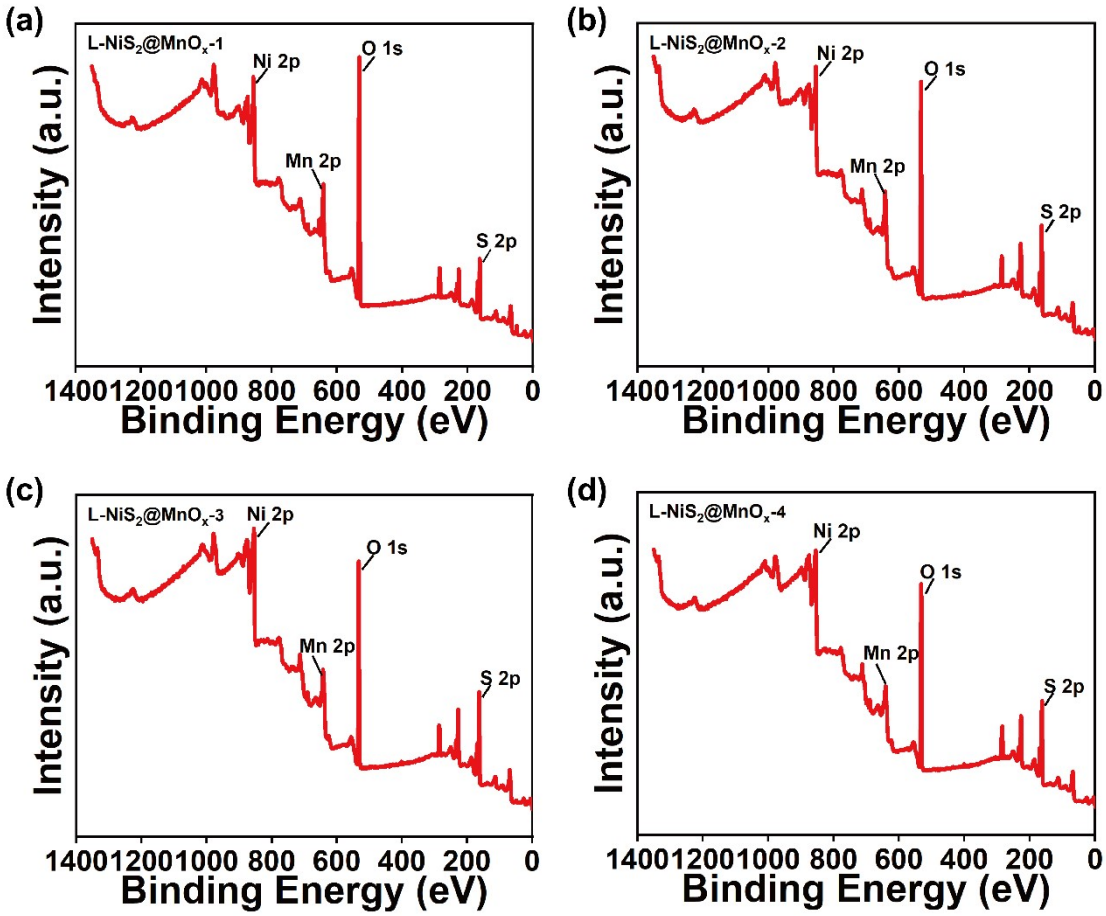

Figure S8. Full XPS spectra of (a) L-NiS_2@MnO_x-1, (b) L-NiS_2@MnO_x-2, (c) L-NiS_2@MnO_x-3, (d) L-NiS_2@MnO_x-4.

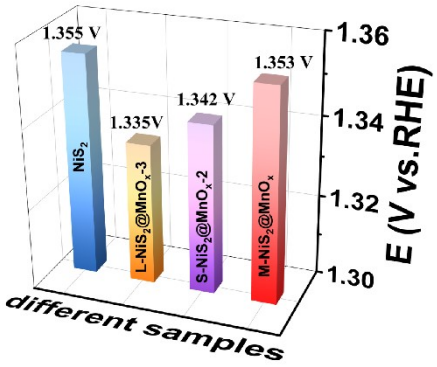

Figure S9. Comparison of potentials required for NiS_2, L-NiS_2@MnO_x-3, S-NiS_2@MnO_x-2 and M-NiS_2@MnO_x to reach a current density of 10 mA cm^{-2}.

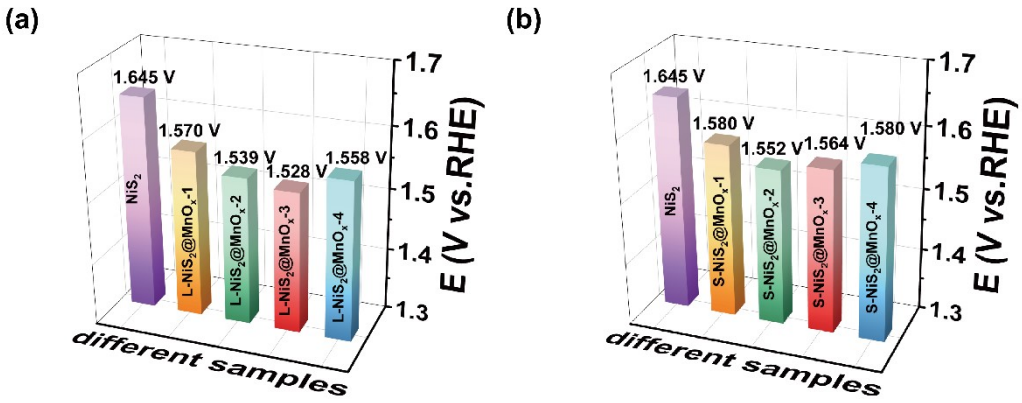

Figure S10. (a) Comparison of potentials required for NiS_2 and L-NiS_2@MnO_x-n to reach a current density of 100 mA cm^{-2}. (b) Comparison of potentials required for NiS_2 and S-NiS_2@MnO_x-n to reach a current density of 100 mA cm^{-2}.

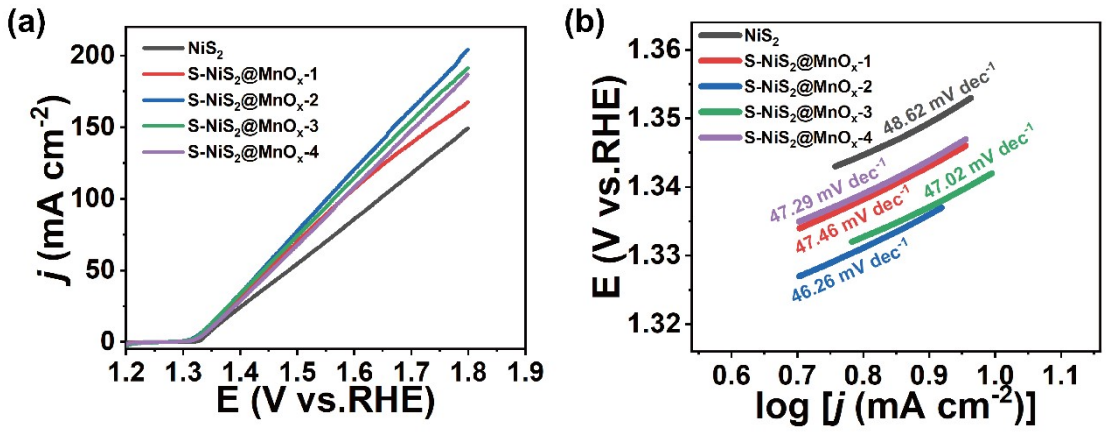

Figure S11. (a) LSV curves of NiS_2 and S-NiS_2@MnO_x-n in the electrolyte of 1.0 M KOH and 0.33 M urea. (b) Tafel plots of NiS_2 and S-NiS_2@MnO_x-n.

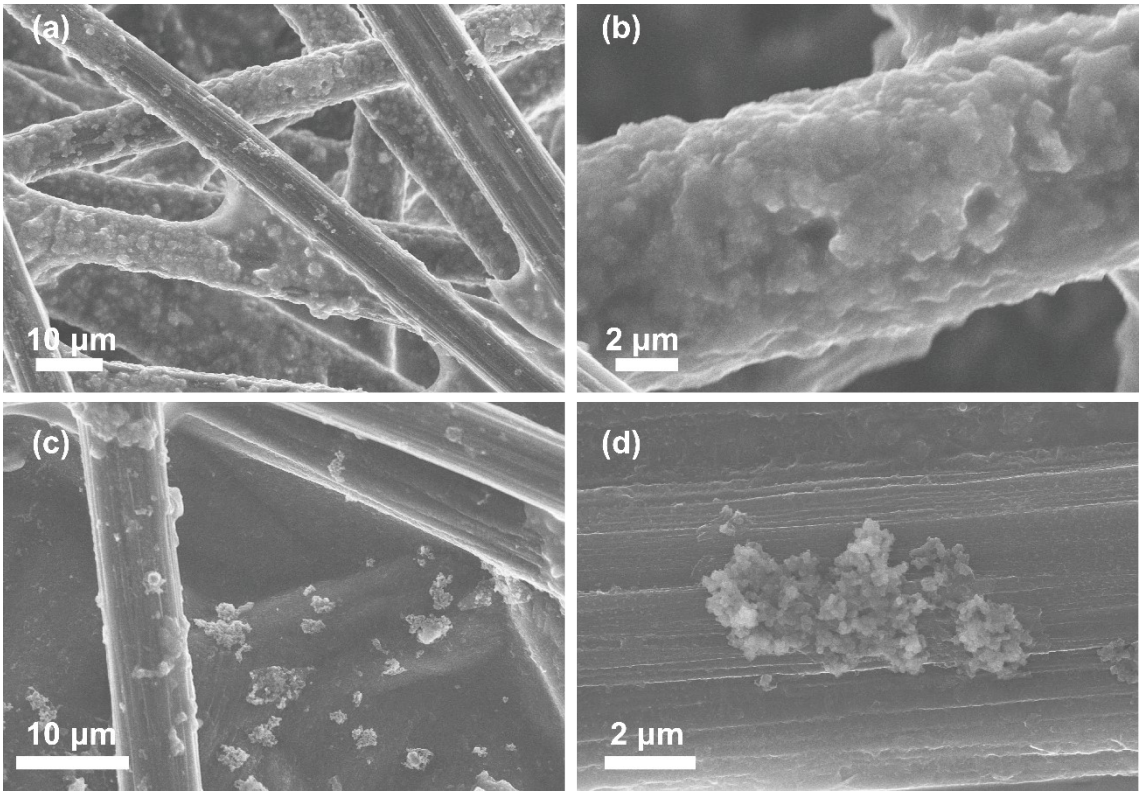

Figure S12. (a, b) SEM images of NiS_2 dripping on carbon paper after UOR test under different scales. (c, d) SEM images of L-NiS_2@MnO_x-3 dripping on carbon paper after UOR test under different scales.

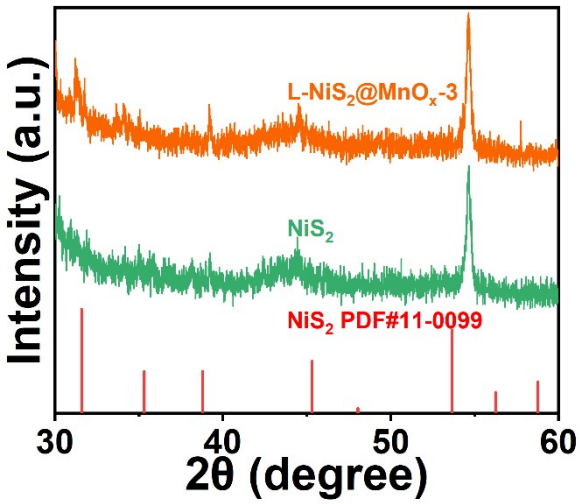

Figure S13. XRD patterns of NiS_2 and L-NiS_2@MnO_x-3 dripping on carbon paper after UOR test.

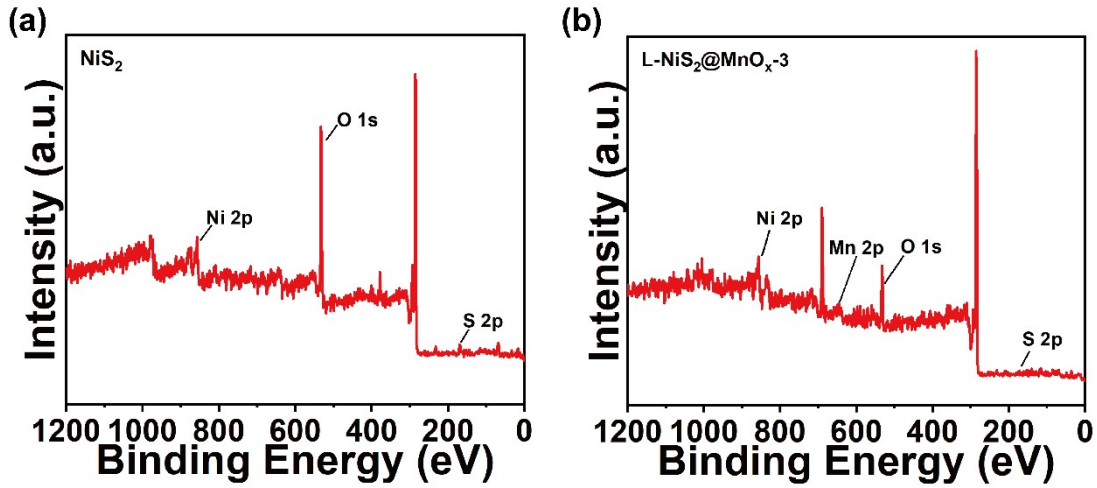

Figure S14. Full XPS spectra of (a) NiS_2, (b) L-NiS_2@MnO_x-3 dripping on carbon paper after UOR test.

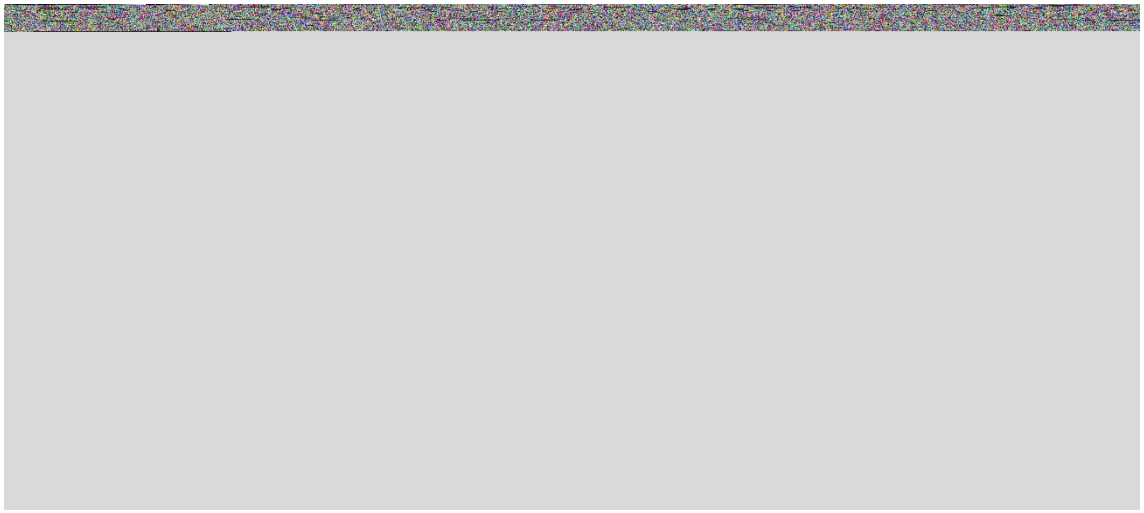

Figure S15. XPS spectra of (a) Ni 2p, (b) S 2p of NiS_2 dripping on carbon paper after UOR test.

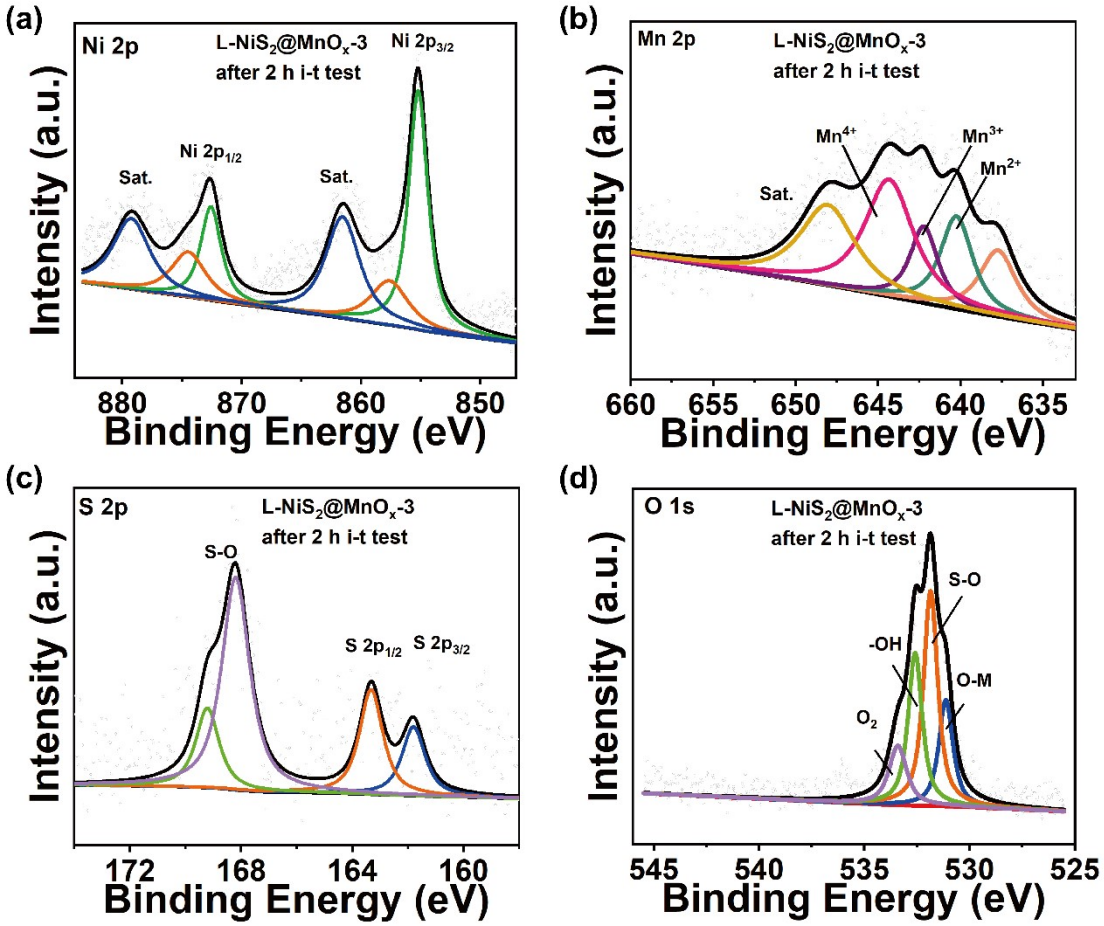

Figure S16. XPS spectra of (a) Ni 2p, (b) Mn 2p, (c) S 2p, (d) O 1s of L-NiS_2@MnO_x-3 dripping on carbon paper after UOR test.

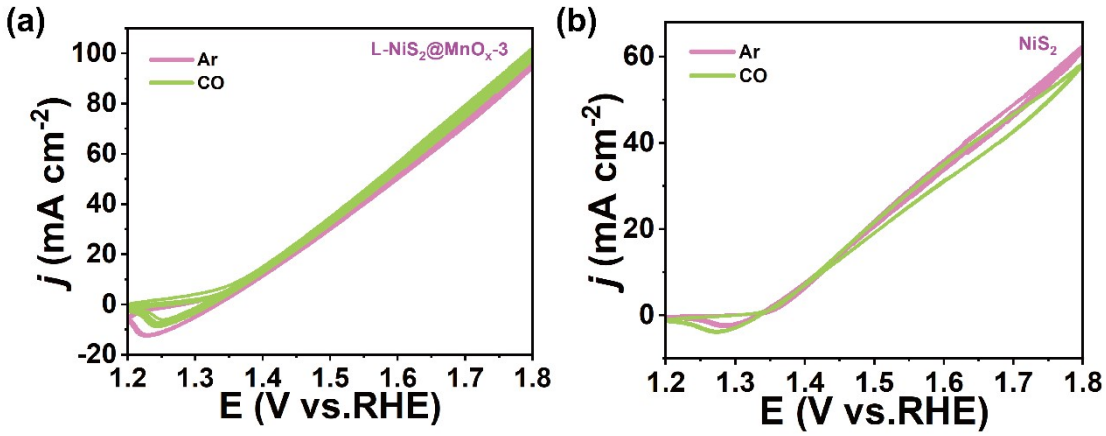

Figure S17. CV curves of (a) L-NiS_2@MnO_x-3, and (b) NiS_2 input Ar and CO electro-oxidation test respectively.

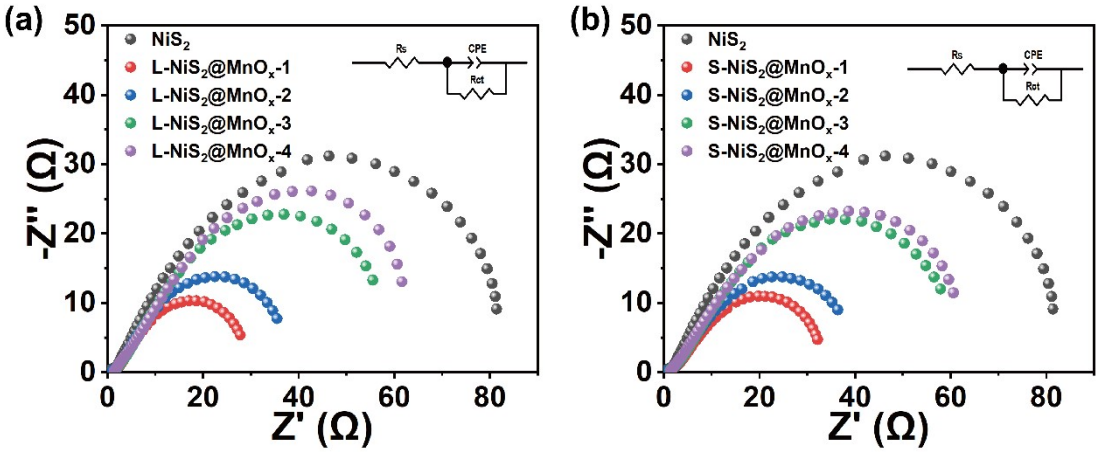

Figure S18. (a) Nyquist plots of NiS_2 and L-NiS_2@MnO_x-n. (b) Nyquist plots of NiS_2 and S-NiS_2@MnO_x-n.

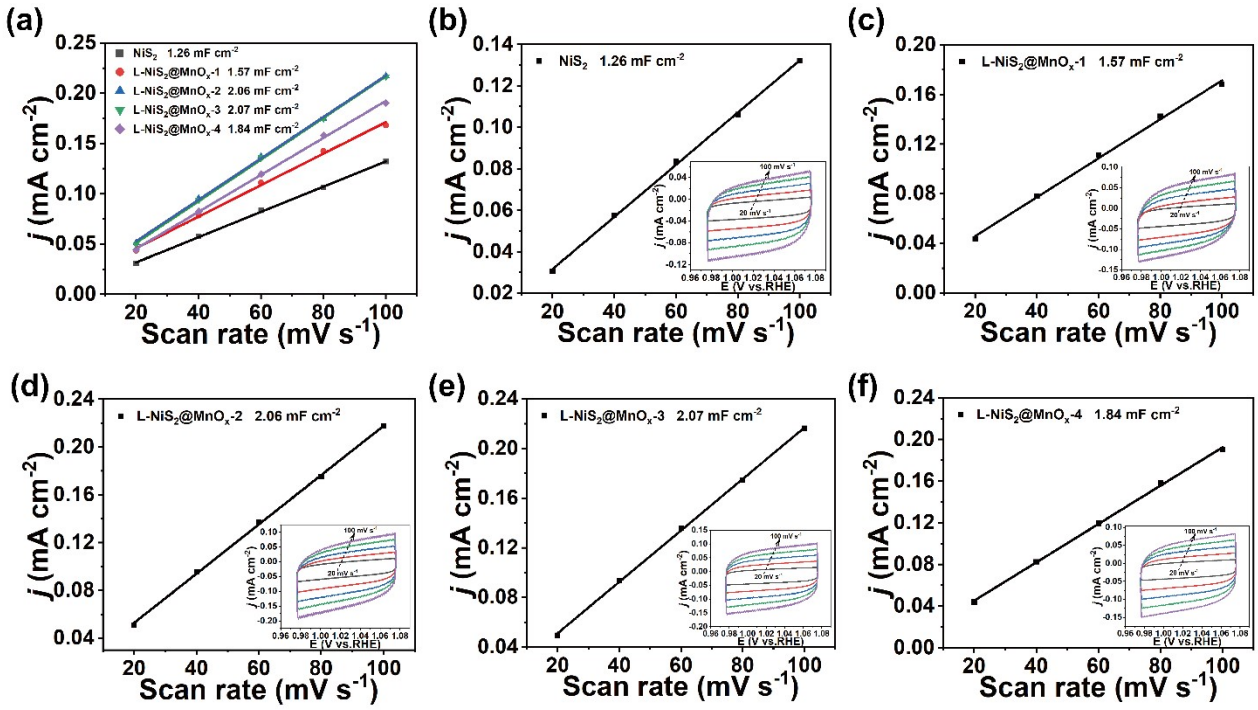

Figure S19. (a) Calculated electrochemical double-layer capacitances for NiS_2 and L-NiS_2@MnO_x. Scan rate-dependent current densities to estimate the C_{dl} of (b) NiS_2, (c) L-NiS_2@MnO_x-1, (d) L-NiS_2@MnO_x-2, (e) L-NiS_2@MnO_x-3, (f) L-NiS_2@MnO_x-4. The insets were the CV cycles measured at the scan rates of 20, 40, 60, 80, and 100 mV s^{-1} in the potential region of 0.975 V–1.075 V (vs. RHE), respectively.

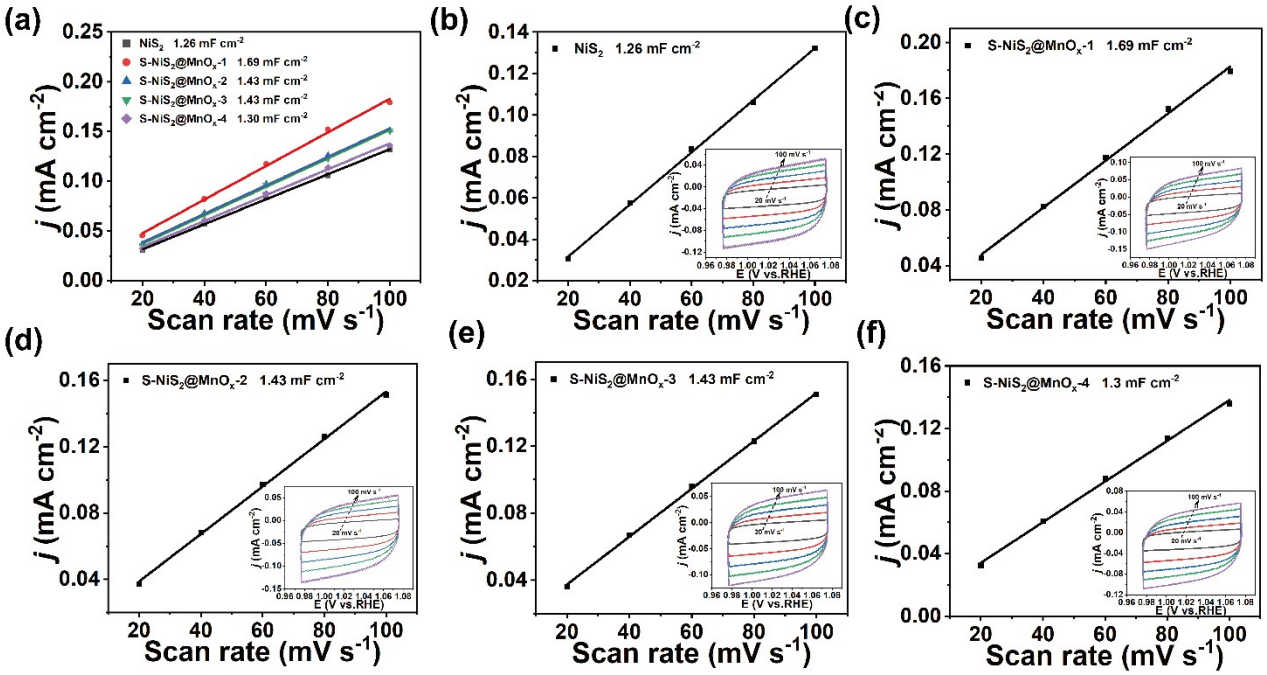

Figure S20. (a) Calculated electrochemical double-layer capacitances for NiS_2 and S-NiS_2@MnO_x. Scan rate-dependent current densities to estimate the C_{dl} of (b) NiS_2, (c) S-NiS_2@MnO_x-1, (d) S-NiS_2@MnO_x-2, (e) S-NiS_2@MnO_x-3, (f) S-NiS_2@MnO_x-4. The insets were the CV cycles measured at the scan rates of 20, 40, 60, 80, and 100 mV s^{-1} in the potential region of 0.975 V–1.075 V (vs. RHE), respectively.

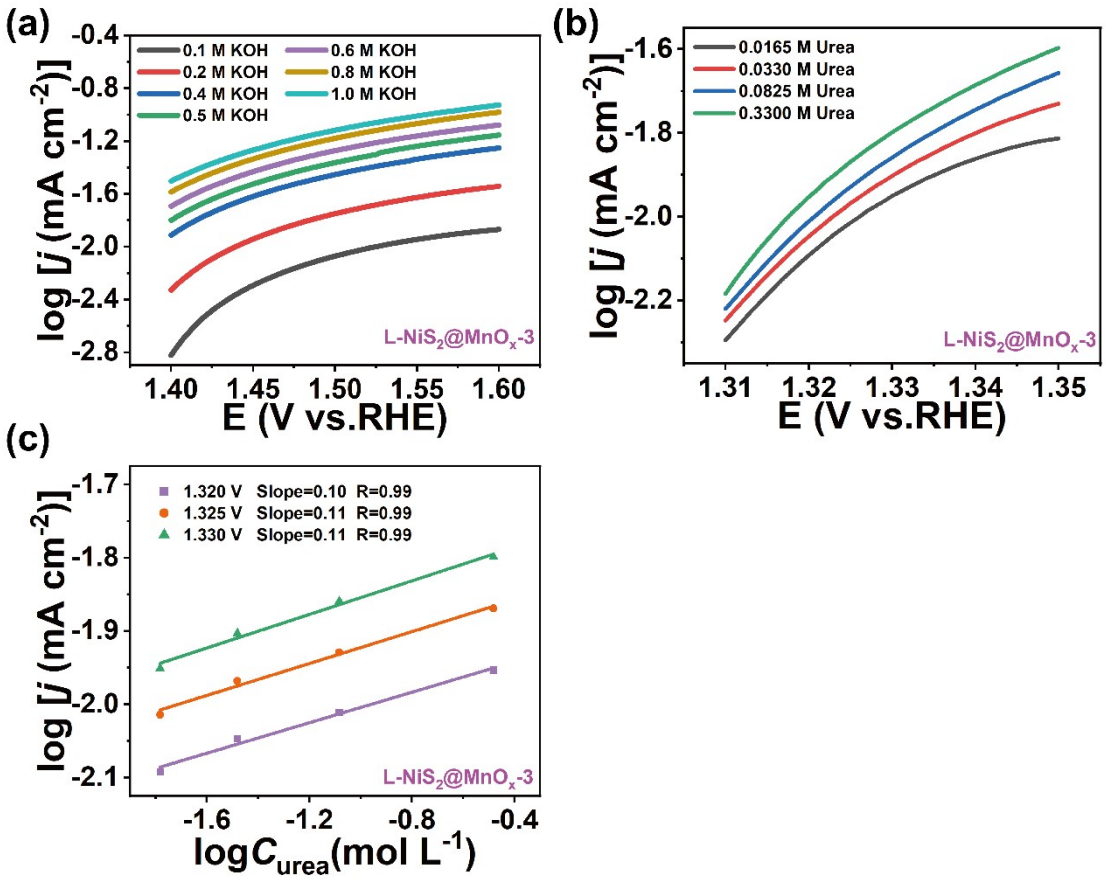

Figure S21. (a) Tafel plots at various KOH concentrations in 0.33 M urea solution at a scan rate of 5 mV s^{-1} under the catalysis of L-NiS_2@MnO_x-3. (b) Tafel plot at various concentrations of urea in 1 M KOH solution at a potential scan rate of 5 mV s^{-1} under the catalysis of L-NiS_2@MnO_x-3. (c) Double logarithmic plot of current density as a function of Urea concentration at constant electrode potentials: 1.320 V; 1.325 V; 1.330 V (vs. RHE). The slopes of the double logarithmic plot at constant electrode potential with a slopes of ~0 showed the reaction order of 0 for urea.

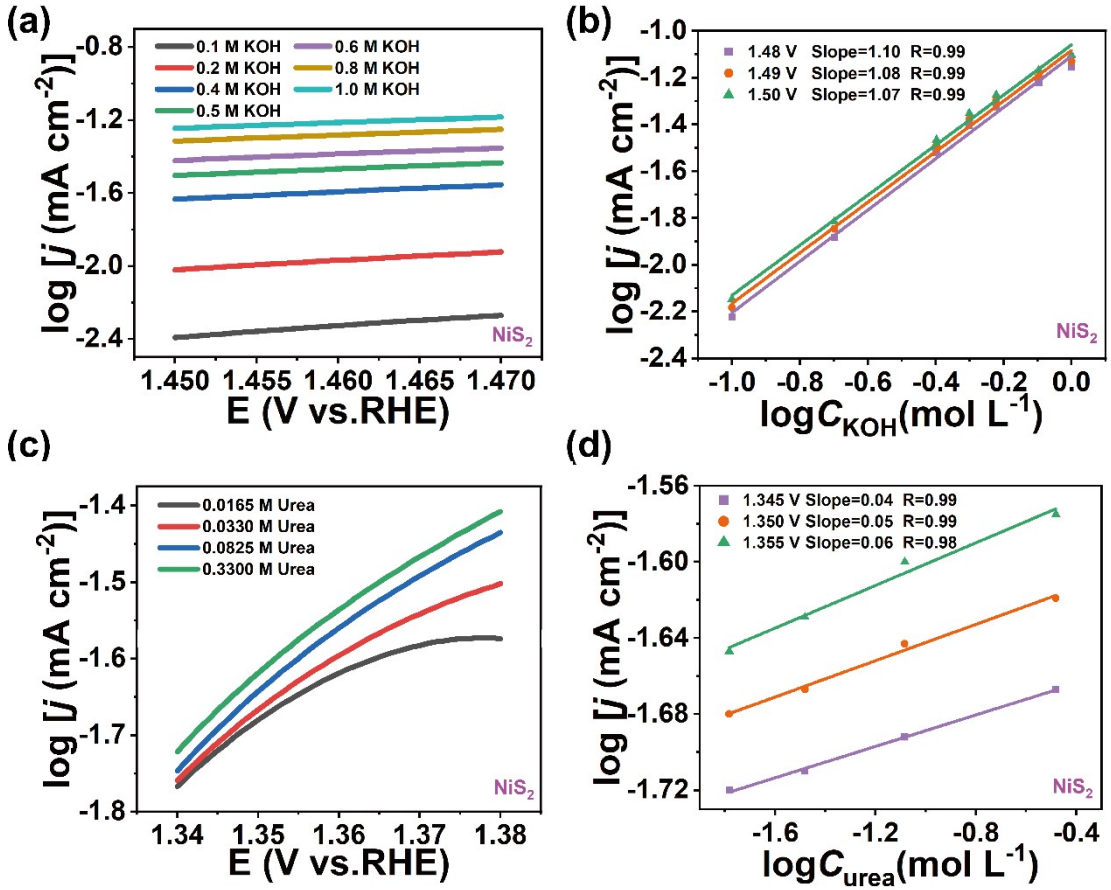

Figure S22. (a) Tafel plots at various KOH concentrations in 0.33 M urea solution at a scan rate of 5 mV s^{-1} under the catalysis of NiS_2. (b) Double logarithmic plot of current density as a function of KOH concentration at constant electrode potentials: 1.48 V; 1.49 V; 1.50 V (vs. RHE). The plots were linear at all tested potentials with slopes of 1, suggesting the reaction order of 1 for OH^- ions. (c) Tafel plot at various concentrations of urea in 1 M KOH solution at a potential scan rate of 5 mV s^{-1} under the catalysis of NiS_2. (d) Double logarithmic plot of current density as a function of Urea concentration at constant electrode potentials: 1.320 V; 1.325 V; 1.330 V (vs. RHE). The slopes of the double logarithmic plot at constant electrode potential with a slopes of ~0 showed the reaction order of 0 for urea.

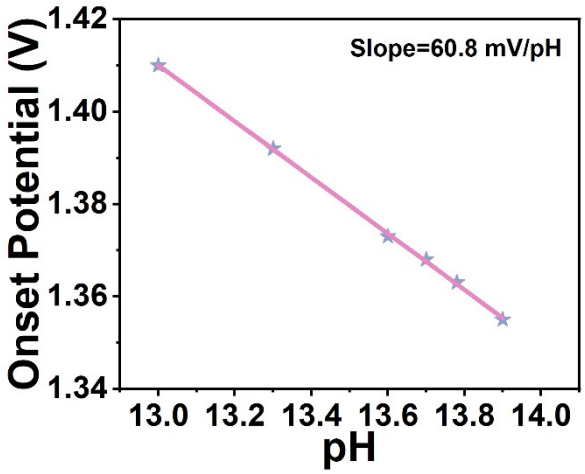

Figure 23. Effect of pH on the onset potential for L-NiS_2@MnO_x-3 catalyst.

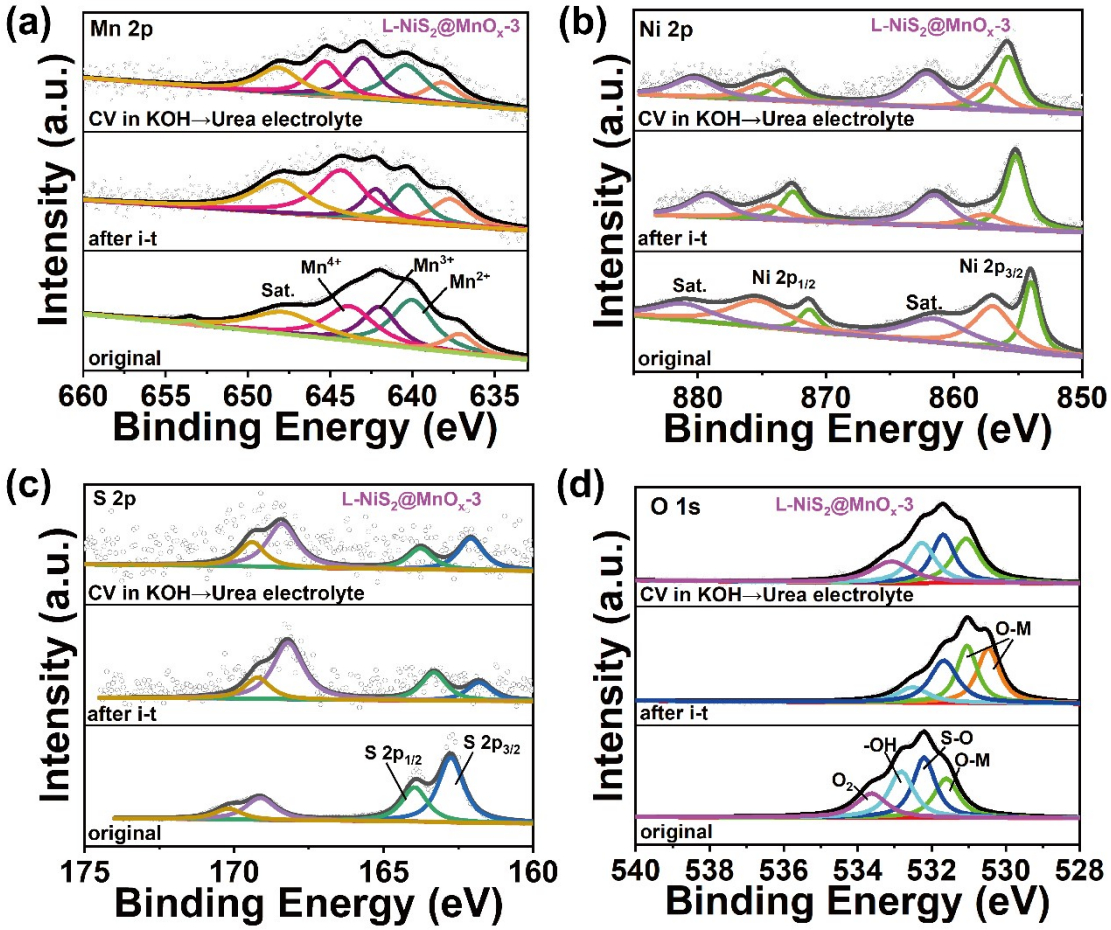

Figure S24. XPS spectra of (a) Mn 2p, (b) Ni 2p, (c) S 2p, (d) O 1s of L-NiS_2@MnO_x.

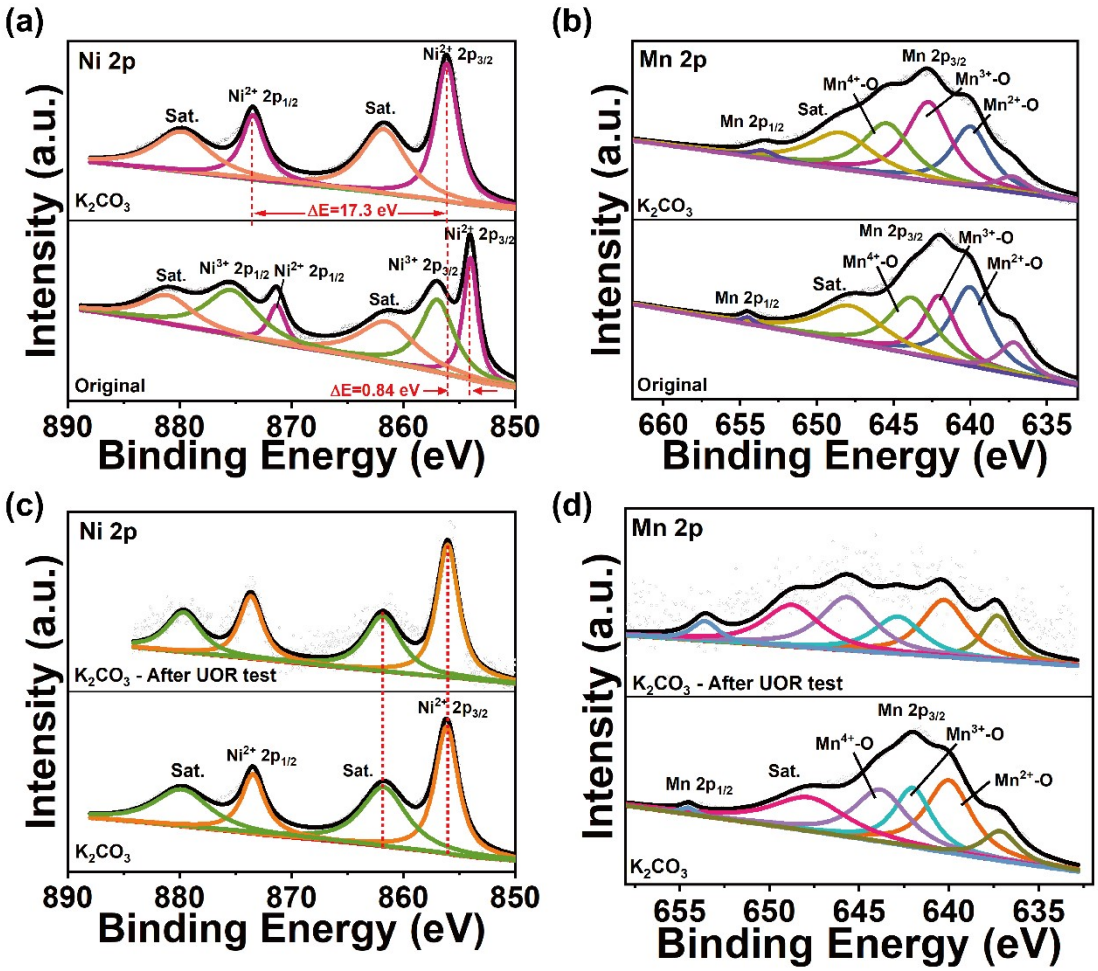

Figure S25. XPS spectra of (a) Ni 2p, (b) Mn 2p of L-NiS_2@MnO_x after soaking in 0.1 M K_2CO_3 for 4 h. XPS spectra of (c) Ni 2p, (d) Mn 2p of L-NiS_2@MnO_x after soaking in 0.1 M K_2CO_3 for 4 h and then performing UOR test.

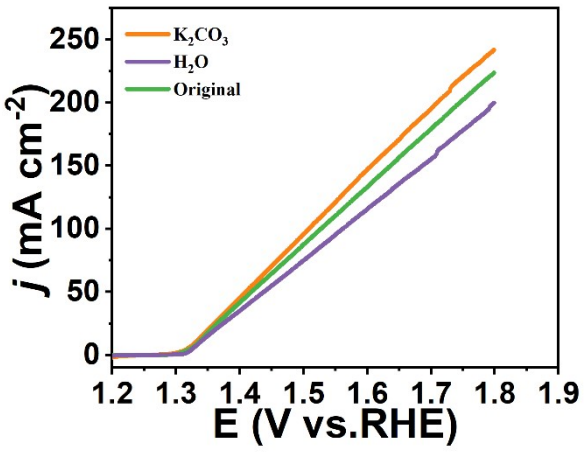

Figure S26. LSV curves of L-NiS_2@MnO_x-3 after soaking in 0.1 M K_2CO_3 and Milli-Q water for 4 h, respectively.

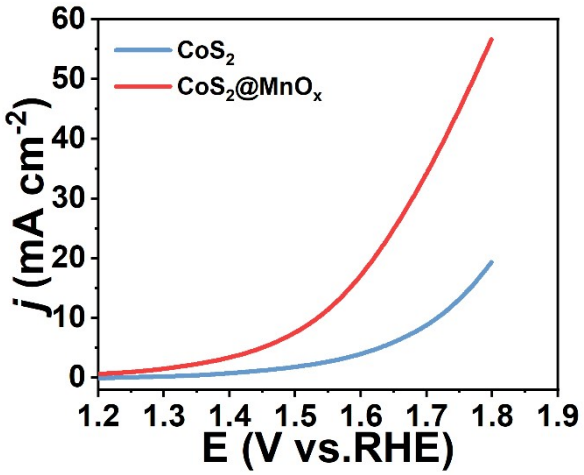

Figure S27. The linear sweep voltammetry (LSV) curves of CoS_2 and $CoS_2@MnO_x$ in the electrolyte of 1.0 M KOH and 0.33 M urea.

Table S1. Ni $2p_{3/2}$ XPS analysis results of NiS_2 and L-NiS_2@MnO_x-n.

Sample	Satellite peak	Ni^{3+}-S	Ni^{2+}-S
NiS_2	861.52	857.00	854.09
L-NiS_2@MnO_x-1	861.41	856.02	853.70
L-NiS_2@MnO_x-2	861.56	857.17	854.18
L-NiS_2@MnO_x-3	861.47	856.96	854.00
L-NiS_2@MnO_x-4	861.19	856.65	853.56
L-NiS_2@MnO_x-3 After 40 min i-t test	861.53	857.60	855.19
L-NiS_2@MnO_x-3 After CV test	862.13	857.22	855.74
L-NiS_2@MnO_x-3 After 12 h i-t test	862.50	860.00	856.00
L-NiS_2@MnO_x-3 (K_2CO_3)	861.74	/	856.12
L-NiS_2@MnO_x-3 (K_2CO_3) After 12 h i-t test	861.83	/	856.03

Table S2. Mn $2p_{3/2}$ XPS analysis results of L-NiS_2@MnO_x-n.

Sample	Satellite peak	Mn^{4+}-O	Mn^{3+}-O	Mn^{2+}-O
L-NiS_2@MnO_x-1	647.35	644.42	642.49	641.04
L-NiS_2@MnO_x-2	647.38	644.10	642.25	640.50
L-NiS_2@MnO_x-3	647.80	643.80	642.00	640.00
L-NiS_2@MnO_x-4	648.42	645.34	642.59	639.90
L-NiS_2@MnO_x-3 After 40 min i-t test	648.04	644.32	642.21	640.23
L-NiS_2@MnO_x-3 After CV test	648.12	645.28	643.01	640.37
L-NiS_2@MnO_x-3 (K_2CO_3)	648.42	645.44	642.71	639.97
L-NiS_2@MnO_x-3 (K_2CO_3) After 12 h i-t test	648.74	645.67	642.83	640.27

Table S3. S 2p XPS analysis results of NiS_2 and L-NiS_2@MnO_x-n.

Sample	S^{6+}-O	S^{4+}-O	$2p_{1/2}$S-Metal	$2p_{3/2}$S-Metal
NiS_2	170.12	169.11	164.00	162.82
L-NiS_2@MnO_x-1	169.58	168.52	164.19	163.00
L-NiS_2@MnO_x-2	170.18	169.12	163.96	162.75
L-NiS_2@MnO_x-3	170.24	169.15	164.22	163.02
L-NiS_2@MnO_x-4	169.75	168.65	163.72	162.52
L-NiS_2@MnO_x-3 After 40 min i-t test	169.21	168.19	163.32	161.80
L-NiS_2@MnO_x-3 After CV test	169.40	168.39	163.77	162.08
L-NiS_2@MnO_x-3 After 12 h i-t test	170.21	168.69	164.34	163.09

Table S4. O 1s XPS analysis results of NiS_2 and L-NiS_2@MnO_x-n.

Sample	O_2	-OH	O-S	O-Metal
NiS_2	533.72	532.95	532.3	531.7
L-NiS_2@MnO_x-1	533.28	532.43	531.80	531.19
L-NiS_2@MnO_x-2	533.56	532.71	532.09	531.49
L-NiS_2@MnO_x-3	533.62	532.82	532.20	531.60
L-NiS_2@MnO_x-4	/	532.90	532.04	531.44/530.85
L-NiS_2@MnO_x-3 After 40 min i-t test	/	532.51	531.67	531.04/530.47
L-NiS_2@MnO_x-3 After CV test	533.08	532.26	531.69	531.07
L-NiS_2@MnO_x-3 After 12 h i-t test	533.08	532.05	531.51	530.86

Table S5. The concentration of Ni and Mn element in the electrolyte after i-t test for 0 h, 3 h, 6 h, 9 h and 12 h.

Time / h	0	3	6	9	12
Ni content / ng mL^{-1}	6.68	7.12	7.18	7.58	7.26
Mn content / ng mL^{-1}	11.02	16.83	18.38	20.32	21.05

Table S6. Comparison of urea electrooxidation performance for several recently reported highly active catalysts

Catalyst	Potential @ 10 mA cm^{-2} (V vs.RHE)	Mass loading (mg cm^{-2})	Electrolyte KOH / urea	Reference
L-NiS_2@MnO_x-3	1.335	0.5	1 M/0.33 M	This work
S-NiS_2@MnO_x-2	1.342	0.5	1 M/0.33 M	This work
M-NiS_2@MnO_x	1.353	0.5	1 M/0.33 M	This work
NiS_2	1.355	0.5	1 M/0.33 M	This work
S-MnO_2	1.33	1.5	1 M/0.50 M	[4]
CoMn/$CoMn_2O_4$	1.32	1.2	1 M/0.50 M	[5]
MnO_2/$MnCo_2O_4$	1.33	1.27	1 M/0.50 M	[6]
Ni-Co-V sulfide	1.33	0.5	1 M/0.33 M	[7]
NP-$Ni_{0.70}Fe_{0.30}$	1.33	0.8	1 M/0.33 M	[8]
$LaNiO_3$	1.39	0.051	1 M/0.33 M	[9]
W-NiS_2/MoO_2@CC	1.30	-	1 M/0.33 M	[10]
β-$NiMoO_4$	1.38	2	1 M/0.50 M	[11]
Ni-MOF@NiO/Ni-2	1.40	-	1 M/0.33 M	[12]
O-NiMoP/NF	1.31	5	1 M/0.50 M	[13]
NiClO-D	1.341	6	1 M/0.33 M	[14]
V_{Ni}-α-$Ni(OH)_2$-4	1.37	0.142	1 M/0.33 M	[15]
VOOH-Ni	1.356	0.5	1 M/0.33 M	[16]
NiSnS	1.36	0.5	1 M/0.33 M	[17]
Ni/Co oxide	1.38	-	1 M/0.33 M	[18]

References

1. S. Zhao, Y. Wang, J. Dong, C.-T. He, H. Yin, P. An, K. Zhao, X. Zhang, C. Gao, L. Zhang, J. Lv, J. Wang, J. Zhang, A. M. Khattak, N. A. Khan, Z. Wei, J. Zhang, S. Liu, H. Zhao and Z. Tang, *Nat. Energy*, 2016, **1**, 12184.
2. S. Rezaee and S. Shahrokhian, *Nanoscale*, 2020, **12**, 16123-16135.
3. K. Ye, G. Wang, D. Cao and G. Wang, *Top Curr Chem*, 2018, **376**, 37642.
4. S. Chen, J. Duan, A. Vasileff and S. Z. Qiao, *Angew. Chem. Int. Ed.*, 2016, **55**, 3804-3808.
5. C. Wang, H. Lu, Z. Mao, C. Yan, G. Shen and X. Wang, *Adv. Funct. Mater.*, 2020, **30**, 2000556.
6. C. Xiao, S. Li, X. Zhang and D. R. MacFarlane, *J. Mater. Chem. A*, 2017, **5**, 7825-7832.
7. Z. Ji, Y. Song, S. Zhao, Y. Li, J. Liu and W. Hu, *ACS Catal.*, 2021, **12**, 569-579.
8. Z. Cao, T. Zhou, X. Ma, Y. Shen, Q. Deng, W. Zhang and Y. Zhao, *ACS Sustain. Chem. Eng.*, 2020, DOI: 10.1021/acssuschemeng.0c04049, 11007–11015.
9. R. P. Forslund, J. T. Mefford, W. G. Hardin, C. T. Alexander, K. P. Johnston and K. J. Stevenson, *ACS Catal.*, 2016, **6**, 5044-5051.
10. S. Ligani Fereja, P. Li, Z. Zhang, J. Guo, Z. Fang, Z. Li, S. He and W. Chen, *Chem. Eng. J.*, 2021, **432**, 134274.
11. K. Hu, S. Jeong, G. Elumalai, S. Kukunuri, J.-i. Fujita and Y. Ito, *ACS Appl. Energy Mater.*, 2020, **3**, 7535-7542.
12. Q. Li, S. Zheng, M. Du and H. Pang, *Chem. Eng. J.*, 2021, **417**, 129201.
13. H. Jiang, M. Sun, S. Wu, B. Huang, C. S. Lee and W. Zhang, *Adv. Funct. Mater.*, 2021, **31**, 2104951.
14. L. Zhang, L. Wang, H. Lin, Y. Liu, J. Ye, Y. Wen, A. Chen, L. Wang, F. Ni, Z. Zhou, S. Sun, Y. Li, B. Zhang and H. Peng, *Angew. Chem. Int. Ed.*, 2019, **58**, 16820-16825.
15. Q. He, Y. Wan, H. Jiang, Z. Pan, C. Wu, M. Wang, X. Wu, B. Ye, P. M. Ajayan and L. Song, *ACS Energy Lett.*, 2018, **3**, 1373-1380.
16. D. Wei, W. Tang, N. Ma and Y. Wang, *Mater. Lett.*, 2021, **291**, 129593.
17. Z. Ji, J. Liu, Y. Deng, S. Zhang, Z. Zhang, P. Du, Y. Zhao and X. Lu, *J. Mater. Chem. A*, 2020, **8**, 14680-14689.
18. H. Xu, Y. Liao, Z. Gao, Y. Qing, Y. Wu and L. Xia, *J. Mater. Chem. A*, 2021, **9**, 3418-3426.